Bioprocess and Biosystems Engineering
https://doi.org/10.1007/s00449-026-03433-4

RESEARCH PAPER

Stabilization of microbial cell population for long-term plasmid production in continuous biomanufacturing

Hannah Sehrt[1] · Juan Andres Martinez[1] · Mathéo Delvenne[1] · Matteo Antognoli[2] · Romain Kinet[3] · Frank Delvigne[1]

Received: 22 July 2026 / Accepted: 22 September 2026
© The Author(s), under exclusive licence to Springer-Verlag GmbH Germany, part of Springer Nature 2026

Abstract
Bacterial cells such as *Escherichia coli* are generally considered insensitive to shear stress in stirred bioreactors, primarily because their small size is assumed to place them below the length scales at which mechanical forces become damaging. This assumption underlies the widespread use of high agitation rates in microbial bioprocesses. However, cellular physiology can strongly modulate this apparent robustness. Metabolic burden associated with high-copy plasmid maintenance and replication is known to alter cell morphology, including increases in cell size and changes in envelope integrity, potentially modifying the mechanical vulnerability of cells. In this study, we investigated the impact of agitation intensity on plasmid-bearing *E. coli* cultivated in continuous mode. Using automated flow cytometry coupled to fluorescent reporters, we observed a rapid and reproducible population collapse in continuous bioreactors operated at standard stirring rates in 1 L bioreactors i.e., 1000 rpm. This collapse occurred despite growth conditions that are classically considered safe for bacterial systems, highlighting that physiological state rather than nominal cell size alone determines sensitivity to mechanical stress. Our results demonstrate that metabolic burden can indirectly expose bacterial populations to shear-related instabilities, challenging standard assumptions in continuous cultivation. Importantly, by accounting for this effect, we developed a robust operating protocol that enables stable continuous cultivation of plasmid DNA-producing cells for more than 100 h. These findings have direct implications for the design and operation of future continuous biomanufacturing processes.

Keywords Replication stress · Cell filamentation · Flow cytometry profiling · Cell population collapse · Plasmid stability · Mechanical stress

Introduction

To produce recombinant proteins or metabolites in *Escherichia coli*, or vaccines for therapeutic applications, plasmid DNA (pDNA) is commonly used as a vector. However, pDNA production remains a challenge, as plasmids within cells can have a negative impact at the cellular and metabolic levels [1]. Particularly critical for a high pDNA productivity are the reductions in growth rate [2–4] and biomass yield [3] caused by the plasmid metabolic load, which can also be amplified by the copy number of the plasmid [4] and when a protein [5, 6] or metabolite is expressed. One of the reasons for the reduced growth rate in plasmid-carrying cells is a morphological change to filamentous cells, which can result from the downregulation of essential cell division proteins [1] and the SOS stress response [1, 7, 8].

The metabolic burden related to plasmid DNA production and the resulting effects influence both the structural [9] and segregational stability [10] of plasmids, which can negatively impact the long-term stability of bioprocesses. Structural instability affects the plasmid sequence and can lead to mutations, whereas segregational instability results in an unequal distribution of plasmids among daughter cells, potentially leading to cells lacking plasmids. Consequently, several strategies have been investigated to enhance controllability and, thus, the stability of plasmid copy number. Early approaches focused on adjusting process parameters such as temperature [11, 12], pH[11], medium composition [13–22] or oxygen [23, 24] to positively influence pDNA

✉ Frank Delvigne
F.Delvigne@uliege.be

1 Terra Research and Teaching Center, Microbial Processes and Interactions (MiPI), Gembloux Agro-Bio Tech, University of Liège, Gembloux, Belgium

2 GSK, Siena, Italy

3 GSK, Rixensart, Belgium

Published online: 01 October 2026

production during bioreactor cultivations. The first genetic modifications to improve plasmid copy number were made over 45 years ago, when pUC19, a plasmid still widely used for high-copy-number production, was constructed from the plasmid pBR322 belonging to the ColE1 family [25]. To further increase copy number, more recent approaches have aimed to exploit the plasmid's native replication control by introducing additional regulatory elements - such as RNAI or RNAII for the pUC19 ori [26, 27] under the control of inducible promoters.

To date, pDNA production has predominantly relied on batch or fed-batch cultivation strategies. Only a limited number of studies have explored chemostat-based approaches, and these have focused primarily on elucidating the influence of specific growth rate on pDNA yield [11, 28]. In this work, we applied a previously developed automated flow cytometry (FC) protocol to map plasmid replication dynamics across the cell population in continuous stirred tank reactors (CSTRs) [29, 30]. This automated FC workflow enables the regular acquisition of population-level snapshots, providing unprecedented insight into the dynamics of key biological processes, such as plasmid replication. To this end, we engineered a constitutively expressed GFP biosensor encoded on the pUC plasmid of interest, such that the reporter is replicated alongside the plasmid itself. This straightforward approach yielded a correlation between cellular GFP fluorescence and plasmid copy number, enabling high-throughput, automated FC-based quantification.

Leveraging this protocol, we investigated the impact of hydrodynamic stress on plasmid retention during continuous cultivation of *E. coli* carrying a high-copy, metabolically burdensome plasmid. Although *E. coli* cells are several orders of magnitude smaller than the Kolmogorov microscale of turbulent eddies in typical stirred-tank bioreactors, and should therefore not be subject to direct mechanical damage from mixing [31, 32], we paradoxically observed a mixing intensity-dependent collapse in plasmid accumulation at the population level. We attribute this sensitivity to the continuous cultivation context, where the selective pressure for growth is inherently stronger and plasmid loss events are more likely to be amplified through clonal expansion of plasmid-free segregants. To disentangle the underlying mechanisms, we conducted a comparative analysis across cultivation systems spanning a wide range of hydrodynamic environments i.e., laminar-flow microfluidics, low-agitation CSTRs, and high-agitation CSTRs. This analysis revealed that cell elongation, a phenotypic indicator of replication stress associated with plasmid over-accumulation, was the primary driver of population collapse. We validated this assumption based on Computational Fluid Dynamics (CFD) simulation and the determination of the Energy Dissipation – Circulation Function (EDCF). Importantly, we demonstrate that reducing agitation speed in the CSTR was sufficient to maintain plasmid retention for over 100 h of cultivation, highlighting the critical and underappreciated role of mechanical stress in long-term plasmid production stability. To continuously monitor the plasmid copy number, a high-copy plasmid with constitutive superfolder GFP (sfGFP) expression was transformed into *E. coli*, and qPCR measurements were performed to validate the fluorescence signal.

Materials and methods

Strain and plasmid

An *E. coli* strain DH5α with the modified plasmid pTHSSe_53 [33] (Addgene plasmid # 109251; http://n2t.net/addgene:109251; RRID: Addgene_109251), were the ampicillin resistance gene was replaced by a kanamycin resistance gene (pTHSSe_53_Kan), was used to investigate the plasmid copy number of a high copy plasmid during continues cultivations. For non-invasive monitoring of plasmid copy number based on automated flow cytometry, a superfolder green fluorescent protein (sfGFP) tag was inserted on the plasmid and expressed under the constitutive promotor pJ23105.

Cultivation medium

For all cultivations, also for the feed medium, mineral media was used containing: 14.6 gL^{-1} K_2HPO_4, 3.6 gL^{-1} $NaH_2PO_4 \cdot 2H_2O$, 2 gL^{-1} Na_2SO_4, 2.47 gL^{-1} $(NH_4)_2SO_4$, 0.5 gL^{-1} NH_4Cl, 1 gL^{-1} $(NH_4)_2$−H−citrate; 5 gL^{-1} glucose (50 gL^{-1} stock solution) and 0.01 gL^{-1} thiamine. The media is supplemented with 11 mL L^{-1} trace element solution, which is composed of the following components in proportionate amounts: 2/11 of 120 gL^{-1} $MgSO_4$, 3/11 of 16.7 gL^{-1} $FeCl_3 \cdot 6H_2O$, 3/11 of 20.1 gL^{-1} EDTA and 3/11 of a metallic trace element solution. The composition of the metallic trace element solution is 0.74 gL^{-1} $CaCl_2 \cdot 2H_2O$, 0.18 gL^{-1} $ZnSO_4 \cdot 7H_2O$, 0.10 gL^{-1} $MnSO_4 \cdot H_2O$, 0.10 gL^{-1} $CuSO_4 \cdot 5H_2O$ and 0.21 gL^{-1} $CoSO_4 \cdot 7H_2O$. As a selection marker 50 mg L^{-1} kanamycin (50 gL^{-1} stock solution) was added to the media. Before the assembly of the media components, the kanamycin, the trace element solution and the thiamine were sterile-filtrated (0.22 µm), the salt solution and glucose solution were heat-sterilized (at 120 °C).

Continuous cultivation

Continuous cultivations were performed in Bionet F1 bioreactor (Bionet, Murcia, Spain) with a working volume of 1 L.

The agitation speed was initially set to 1000 rpm. For specific experiments the agitations speed was decreased to 780 rpm, which is mentioned for the respective cultivations. Based on experiments conducted in a smaller, unbaffled bioreactor system, in which no loss of GFP fluorescence was observed (see Supplementary Data 4), an equivalent agitation speed for the Bionet system was determined using Kolmogorov scale calculations. To prevent flooding at the impeller, the aeration was set to 1 vvm for cultivation at 1000 rpm and 0.8 vvm for cultivation at 780 rpm. The temperature was set at 37 °C and the pH control was set at 7 (control solutions: 2 M NAOH, 25% H_3PO_4). Bioreactor cultivations started with the batch phase until complete consumption of glucose, followed by the chemostat experiment, where feed media containing 5 gL^{-1} glucose was fed. Unless otherwise specified, the dilution rate during the continuous cultivation was set to 0.1 h^{-1}. *E. coli* was precultured in 1 L flask (100 ml working volume) overnight at 37 °C and 150 rpm shaking speed. The same mineral medium, containing 5 gL^{-1}, was used for the preliminary cultures, as described in "Cultivation Medium". The bioreactor was inoculated with an initial OD_{600nm} of ~0.3.

During continuous cultivation, cells with different fluorescence levels, as measured by flow cytometry, were sampled for cultivation in microfluidic chambers. For this purpose, 1 mL of cell suspension was taken, mixed with 1 mL 50% (w/w) glycerol, and stored at -80 °C until use.

Microfluidic cultivation and time lapse microscopy

E. coli cells were cultivated inside PDMS-glass based microfluidic single-cell cultivation (MSCC) chips for monolayer growth of colonies provided by Alexander Grünberger's lab [34]. Two different chip designs were used to follow growing colonies over time: 90 µm x 120 µm x 778 µm–80 µm x 90 µm x ~ 700 µm. The media used was the same as described above, but before use, the media was filtered (0.22 µm). The preculture was performed in the same way as for the bioreactor cultivation, except that a smaller volume was used (100 ml shaker with a working volume of 10 ml). The chambers were inoculated with cells by flushing the chip with a cell suspension diluted to a OD_{600nm} of ~0.1. At least three cultivation chambers were selected manually to follow the growth of the colonies.

For the time lapse microscopy, images were taken using a Nikon Eclipse Ti2-E inverted automated epifluorescence microscope (Nikon Eclipse Ti2-E, Nikon France, France) equipped with aDS-Qi2 camera (Nikon camera DSQi2, Nikon France, France), a 100× oil objective (CFI P-Apo DM Lambda 100× Oil (Ph3), Nikon France, France). The GFP-3035D cube (excitation filter: 472/30 nm, dichroic mirror: 495 nm, emission filter: 520/35 nm, Nikon France, Nikon) was used to measure GFP. The phase contrast images were recorded with an exposure time of 300 ms and an illuminator's intensity of 30%. The GFP fluorescence images were recorded with an exposure time of 200 ms and an illuminator's intensity of 2% (SOLA SEII, Lumencor, USA). Phase contrast images were acquired every 5 min while GFP fluorescence was measured every 20 min. The optical parameters and the timelapse were managed with the NIS-Elements Imaging Software (Nikon NIS Elements AR software package, Nikon France, France).

Microscopy images from microfluidic cultivations and microscopy images taken during bioreactor cultivations were analyzed as follows. First, the images were exported in '.tiff' files using the NIS-Elements Imaging Software (Nikon NIS Elements AR software package, Nikon France, France). Then, they were preprocessed (normalization, stabilization, cropping, etc.) using a custom-made Python pipeline and Fiji/ImageJ (All relevant code and explanations are available at https://gitlab.uliege.be/mipi/published-software/2024-fitnessentropycompensation/-/tree/main/supplementary_code/Microfluidics_Analysis?ref_type=heads; Commit ID: 0707e64b). The cell segmentation was performed on phase contrast images using a custom-made Python code based on cellpose library (version 0.7.1) [35, 36] with the trained model of Dimalis (https://github.com/Helena-todd/Dimalis, commits 26 Jul 2023, ID: 96ac2c8). Masks images of segmented cells were corrected manually using Fiji/ImageJ before tracking using the Fiji/ImageJ plugin TrackMate (version 7.11.1) [37, 38] with the "Label image detector" and the "Overlap tracker" options (precise IuO calculation, min. IuO = 0.1 and scale factor = 1.1). Singles-cells data and lineages were then exported as tables and further analyzed.

Single-cell plasmid copy number quantification by qPCR

For the quantification of pDNA and the determination of the single-cell plasmid copy number (PCN), 5 mL cell suspension were sampled during bioreactor cultivations at different fluorescence levels. The cell suspensions were centrifuged at 5000 rpm for 10 min, and the cell pellets were stored at -80 °C until analysis. The pellets were then resuspended in purified water to a concentration of 5 gL^{-1}, and mechanical cell lysis was performed using the FastPrep-24 bead beating system (Fisherbrand Bead Mill 24). FastPrep-24 tubes containing Lysing Matrix B (0.1-mm silica beads) were loaded with 1 mL of the cell suspension. The instrument was operated for 6 cycles of bead beating, each lasting 60 s at 6.5 ms^{-1}.

Next, quantitative PCR (qPCR) was used to quantify both pDNA and genomic DNA (gDNA) (detailed cycling program available in Table S2). A mix of primers amplifying

specific sequences from both the *E. coli* genome and the pUC19 plasmid was employed. Specifically, primers targeting a portion of the pUC19 origin of replication (ColE1) and the *E. coli* fumC gene (assumed to be present as a single copy per cell) were used (the exact primer sequences are listed in Table 1). Calibration curves for both the genomic and plasmid targets were generated using in-house standards with known pDNA and gDNA copy numbers. Negative controls were also included in duplicate. Based on these calibration curves, the number of pDNA and gDNA molecules was determined, and the average single-cell PCN was calculated according to Eq. 1.

$$PCN = \frac{number\ of\ pDNA\ molecules}{number\ of\ gDNA\ molecules} \quad (1)$$

The determination of pDNA was done by the company GSK groups of companies (Rixensart, Belgium).

Estimation of mechanical stress: EDCF computation and CFD simulations

Computational fluid dynamics (CFD) simulations were performed to characterize the hydrodynamic environment of the baffled stirred-tank bioreactor and to provide consistent descriptors of mixing intensity for interpreting shear-related biological effects. The objective was not to directly predict cell damage, but to quantify flow-derived quantities i.e., an energy dissipation and circulation function (EDCF), for use within established shear-damage frameworks [39, 40]. For this purpose, the flow field was modeled using a steady-state Multiple Reference Frame (MRF) approach to represent rotation of the Rushton disk turbine with 6 blades (RDT6). The presence of baffles suppresses large-scale swirl and promotes statistically steady turbulent conditions, consistent with standard practice for stirred-tank CFD. The fluid was assumed Newtonian, with physical properties equivalent to water, and the governing equations were solved using a finite-volume approach in ANSYS Fluent (release 24.2).

The computational domain was discretized with a polyhedral mesh comprising approximately 2 million elements over a 1 L working fluid volume, corresponding to an average element size of 0.8 mm. Inflation (boundary) layers were applied to the impeller and vessel wall surfaces to better resolve near-wall turbulence and impeller power transmission.

Table 1 Primers used for the qPCR analyses

Primer name	Sequence
pDNA_ColE1_1	GGCGGTGCTACAGAGTTCTT
pDNA_ColE1_2	TTTGGTATCTGCGCTCTGCT
pDNA_ColE1_3	TGTTTGCCGGATCAAGAGCT
gDNA (e.coli)_1	AGGCGGCGGATGAAGTACT
gDNA (e.coli)_2	AGCCGGTCTGCCAGATAGC
gDNA (e.coli)_3	CAGGACAGCATGACGACGAATTCCC

Turbulence was described using the k–ω Shear Stress Transport (SST) model, selected for its ability to capture shear-dominated and rotation-influenced flows typical of stirred tanks. A single turbulence model was applied consistently across all operating conditions to ensure comparability of results.

The local turbulent energy dissipation rate (ε) was extracted from the turbulence model solution. A characteristic value, εimp, was defined as the volume-averaged dissipation rate within the impeller swept volume, following the approach recently reported [41].

The Kolmogorov length scale was estimated as:

$$\eta = \left(\nu^3/\varepsilon\right)^{(1/4)} \quad (2)$$

where ν is the kinematic viscosity. This scale represents the size of the smallest turbulent eddies and provides a reference for comparing flow structures with the characteristic size of biological entities.

The circulation time (t_c) was estimated from the impeller pumping capacity as:

$$t_c = V/Q \quad (3)$$

where V is the reactor volume and Q is the pumping flow rate of the impeller.

A combined hydrodynamic stress metric, the Energy Dissipation Circulation Function (EDCF) was defined as:

$$EDCF = \varepsilon_{imp}/t_c \quad (4)$$

This metric captures both the intensity of hydrodynamic stress and the frequency of exposure, describing the intermittent stress experienced by the average *E. coli* population as cells circulate through high- and low-dissipation zones of the reactor [40].

The flow was assumed incompressible and isothermal and was described by the Reynolds-averaged Navier–Stokes (RANS) equations. Mass conservation is expressed as $\nabla \cdot u = 0$ and momentum conservation, with closure provided by the Boussinesq approximation, is expressed as:

$$\rho\left(u \cdot \nabla u\right) = -\nabla p + \eta\nabla^2 u - \nabla \cdot \left(\rho u' u'\right) \quad (5)$$

where ρ is the fluid density (kg m^{-3}), u is the velocity vector ($m.s^{-1}$), p is the pressure (Pa), and η is the dynamic viscosity (Pa.s). The term ρ u′u′ represents the Reynolds stress tensor arising from turbulence.

The resulting flow solution provides the spatial distribution of velocity and turbulence quantities used to interpret

the effect of mixing intensity on population dynamics. Simulations were carried out using the native GPU solver on an NVIDIA RTX 6000 Ada Generation GPU (52 GB VRAM), which enabled full simulation turnaround within a single day.

Results

Calibration of an automated FC pipeline for tracking plasmid replication process in cell populations

Identifying reliable single-cell proxies for key biological processes is a critical prerequisite for characterizing cell population dynamics [42, 43]. In the context of plasmid bioproduction, we addressed this need by developing an automated flow cytometry (FC) protocol to monitor population-level responses to plasmid replication stress. To this end, we engineered a high-copy-number plasmid based on the pUC19 origin of replication, carrying a sfGFP reporter under the control of a constitutive promoter, in *Escherichia coli* DH5α. Under this design, each plasmid copy should produce a stoichiometric amount of sfGFP, providing a quantitative single-cell fluorescence proxy for plasmid content (Fig. 1A). To establish a quantitative relationship between fluorescence and plasmid copy number (PCN), we performed a series of continuous cultivation experiments combining automated FC with sparse off-line sampling at various points during the process and upon reaching a constant fluorescence signal. The mean cellular sfGFP level exhibited a strong correlation with PCN ($R^2 = 0.92$), following a hyperbolic, saturation-type relationship (Fig. 1B). This saturation behavior at high plasmid content could reflect the increasing metabolic burden associated with plasmid over-accumulation, which may limit further sfGFP synthesis, represented by GFP_{max} upon fitting to a saturation-type equation (Fig. 1B). We further verified that sfGFP expression itself did not impose any additional metabolic burden beyond that already associated with plasmid replication stress (Supplementary Information, Fig. S1).

Automated FC profiling of cell population dynamics reveals a collapse event during pDNA production

Using automated FC, we tracked the dynamics of the sfGFP tag in a chemostat at a dilution rate of 0.1 h^{-1}, taking regular snapshots of the fluorescence distribution every 12 min (Fig. 2A). Following the onset of continuous cultivation, we observed a gradual decline of the GFP-positive subpopulation, which was progressively replaced by GFP-negative cells (Fig. 2B, C). By the end of the continuous cultivation phase, the GFP-negative subpopulation dominated, accounting for 97% of the population.

The loss of fluorescence, leading to the emergence of a GFP-negative population, represents an irreversible transition. Even under no-shear-stress conditions, such as in

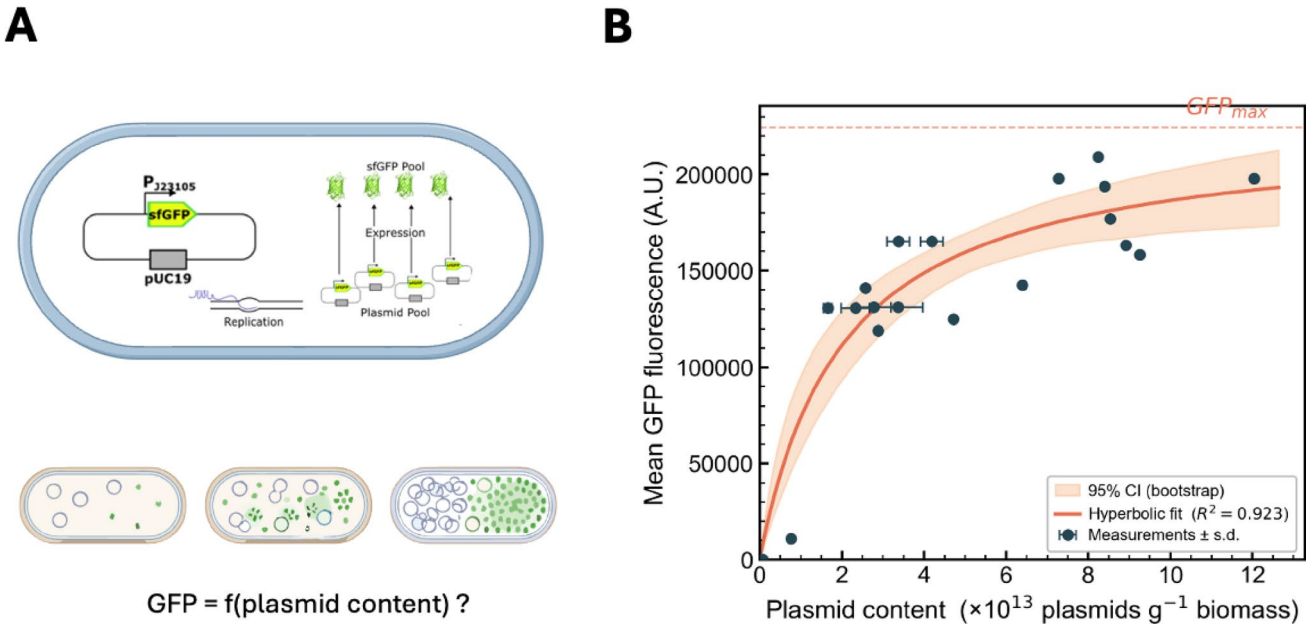


Fig. 1 Development of a GFP reporter for monitoring plasmid accumulated based on FC. **A** Monitoring of the plasmid copy number (PCN) during continuous cultivation using a high-copy plasmid with a pUC19 origin of replication, expressing GFP constitutively (promoter: pJ23105). The plasmid was transformed into *E. coli* DH5α cells to correlate the fluorescence level with the PCN content. To verify the correlation between PCN and mean fluorescence, samples from multiple bioreactors at different fluorescence levels were analyzed via qPCR. **B** Correlation between plasmid per biomass content determined by qPCR and fluorescence level determined based on automated flow cytometry

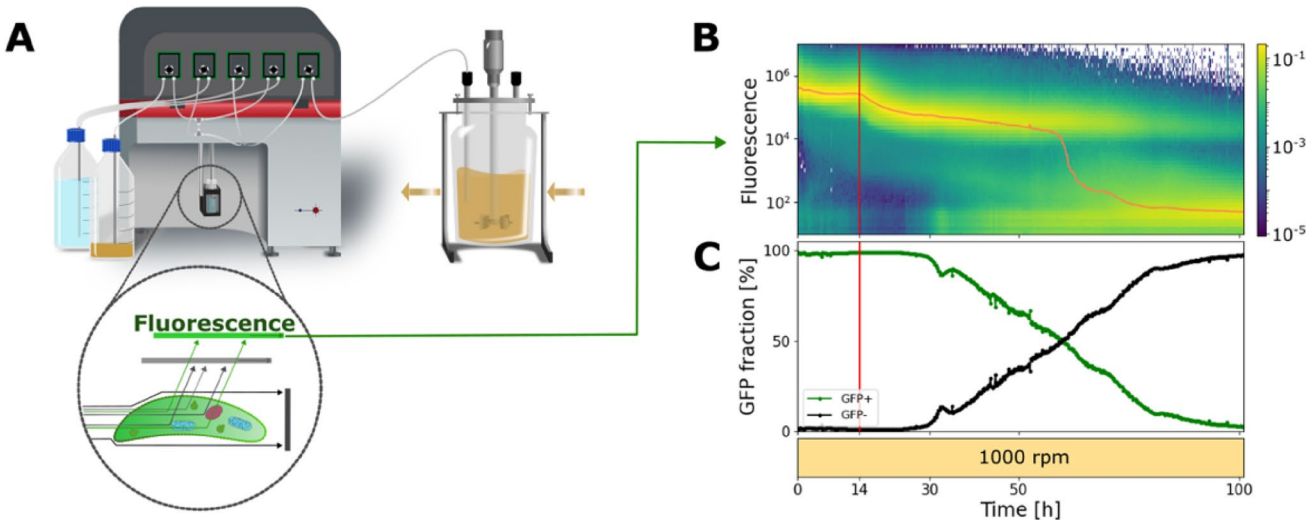


Fig. 2 Automated flow cytometry is used to capture the dynamics of plasmid replication in a cell population during continuous cultivation. **A** Flow cytometer is connected to a continuous bioreactor, taking automated samples every 12 min to analyze the fluorescence level of the cell population inside the bioreactor. **B** Snapshots of measured fluorescence are displayed in a density plot over time for the batch cultivation and the continuous cultivation (after the horizontal red line), with a constant stirring speed of 1000 rpm and a dilution rate of 0.1 h^{-1}. The trend of the median fluorescence is shown as a fine red line. **C** Trend of the positive and negative fractions of cells expressing GFP (threshold = 10^4)

microfluidic cultivation, cells do not revert to the GFP-positive state but instead maintain the physiological state acquired in the bioreactor. Microfluidics cultivation revealed that the GFP-negative subpopulation exhibits a higher specific growth rate, suggesting that the loss of fluorescence and the associated decrease in plasmid copy number, confers a selective growth advantage under continuous cultivation. (Supplementary Information, Figure S2).

However, in the chemostat, a complete loss of the plasmid is unlikely due to the presence of kanamycin. Together, these arguments suggest that the GFP-negative phenotype arises not from plasmid loss, but from genetic alterations that alleviate the metabolic burden while preserving plasmid inheritance [44]. But even when the transfer of plasmids to daughter cells is ensured by selection pressure, the metabolic burden can also be reduced by influencing structural plasmid stability. Due to difficulties in sequencing the entire plasmid after the loss of the GFP signal, two main parts of the plasmid i.e., the *sfGFP* gene and the kanamycin resistance gene, were verified by PCR for bioreactor samples at different GFP levels. At the end of the cultivation, when 0% of the cells were GFP-positive, *sfGFP* was not detectable in the PCR product. For the kanamycin resistance gene, the primers bound successfully, but the PCR product was smaller than expected. (Supplementary Information, Figure S3 and Table S1). Since the kanamycin resistance gene is essential for survival under selection pressure, it is more likely that mutations occur in the plasmid to reduce the metabolic burden [1, 45, 46].

Increasing stirrer speed triggers population collapse during continuous pDNA production

The population collapse observed in the CSTR experiment was accompanied by a visible change in medium color and foam formation, both indicative of cell lysis. To test this hypothesis, we conducted a series of continuous cultivations at varying stirrer speeds. (Fig. 3A). Surprisingly, our results revealed that stirrer speed has a significant impact on population stability. At a stirrer speed of 780 rpm, the GFP-positive subpopulation dominated (>98%) and a stable population profile was observed for over 100 h (Fig. 3B). In contrast, increasing the stirrer speed to 1000 rpm resulted in a rapid collapse of the population. We observed marked differences in cell morphology depending on the stirrer speed (Fig. 3C and D). Specifically, cultures grown at 780 rpm displayed pronounced heterogeneity in cell size, including large, highly fluorescent cells (Fig. 3E and F). In contrast, cultures grown at 1000 rpm exhibited a more uniform and classical *E. coli* morphology with reduced heterogeneity (Fig. 3E). These findings suggest that stirrer speed clearly influences population structure and dynamics, particularly in relation to cell size and plasmid retention. This hypothesis will be further explored in the next section through cultivation experiments conducted under low-shear conditions in microfluidics.

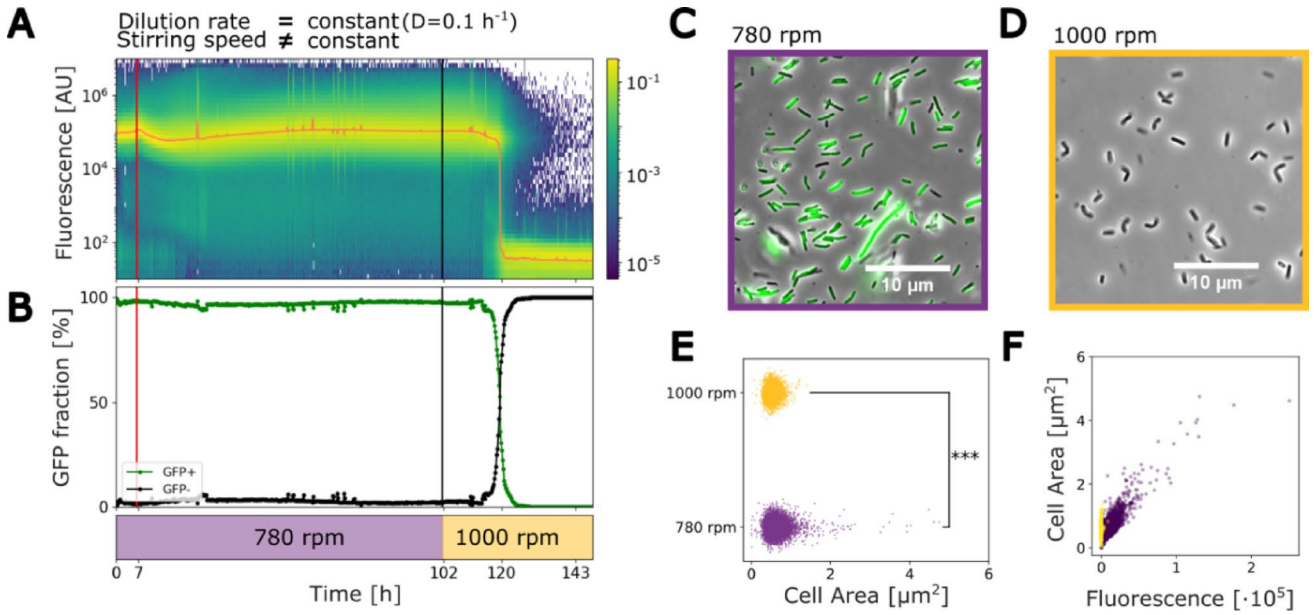


Fig. 3 Increasing stirring speed during continuous cultivation induces the collapse event. **A** Fluorescence density plot of cultivated *E. coli* DH5α cells harboring a high-copy plasmid expressing GFP constitutively, with a stirring speed of 780 rpm for the first 102 h, followed by 1000 rpm for 41 h at a dilution rate of 0.1 h^{-1}. The trend of the median fluorescence is shown as a fine red line. **B** Trend of the positive and negative fractions of cells expressing GFP (threshold = 10^4). Analysis of microscopy images during continuous cultivation at **C** 780 rpm and **D** 1000 rpm. For each condition, 10 images were taken, and fluorescence intensity and **E** cell area were measured for each cell, as well as the correlation between cell area and fluorescence level (**F**). To assess statistical *significance*, *an F-test was performed first*, *followed by a T-Test*

Cell filamentation is observed under low shear stress environment

As detailed in the previous section, stirring rate in bioreactor appears to influence cell size distribution and population dynamics during pDNA production and expression in *E. coli*. To go further, we implemented a system working based on diffusion of the nutrients, without the need for mechanical stirring. We conducted experiments using a Microfluidic Single-Cell Cultivation (MSCC) device [47]. This platform consists of an array of 2D cultivation chambers with open ends, enabling continuous perfusion of fresh medium and removal of spent medium (Fig. 4B). Due to the chamber design, flow within the MSCC device is predominantly laminar, effectively eliminating mechanical stirring as a variable. We performed a series of cultivations in the MSCC and monitored microcolony development over time (Fig. 4C). A high degree of variability was observed between chambers, as shown by fluorescence microscopy images (Fig. 4A). This variability was largely driven by the emergence of slow-growing, highly fluorescent, and significantly enlarged cells (Fig. 4E–I). Some of these cells reached sizes up to 45 µm i.e., well beyond the typical cell dimensions observed in stirred-tank bioreactors and the average cell size of *E. coli* (~3 µm) [48]. The enlargement of cells towards filamentation is a typical stress symptom, in which cell division is disrupted and cells can reach 10–50 times their normal size [45, 49]. In line with the Kolmogorov theory discussed previously, these findings suggest that low-shear environments foster the emergence of larger cells with high pDNA content. This observation aligns with phenomena associated with metabolic burden and cell filamentation, wherein high plasmid copy number or expression load impairs cell division, leading to filamentous growth [50]. Notably, these filamentous cells exhibited markedly reduced growth rates, which in turn affected the expansion dynamics of entire microcolonies. In chambers where filamentous cells appeared early, overall microcolony growth was delayed (Fig. 4C and E). Taken together, these results indicate that the intensity of mixing during pDNA production can significantly impact population structure and dynamics.

Decreasing stirring speed allows for the stabilization of cell population for the continuous bioproduction of pDNA

Based on the data accumulated so far, we concluded that reducing the mixing intensity promotes the emergence of larger cells with elevated pDNA content. To further explore this relationship under continuous cultivation, we performed chemostat experiments at a stirrer speed of 780 rpm while progressively increasing the dilution rate to enhance process productivity. The experiment was carried out over 120 h, during which a remarkably stable population profile was

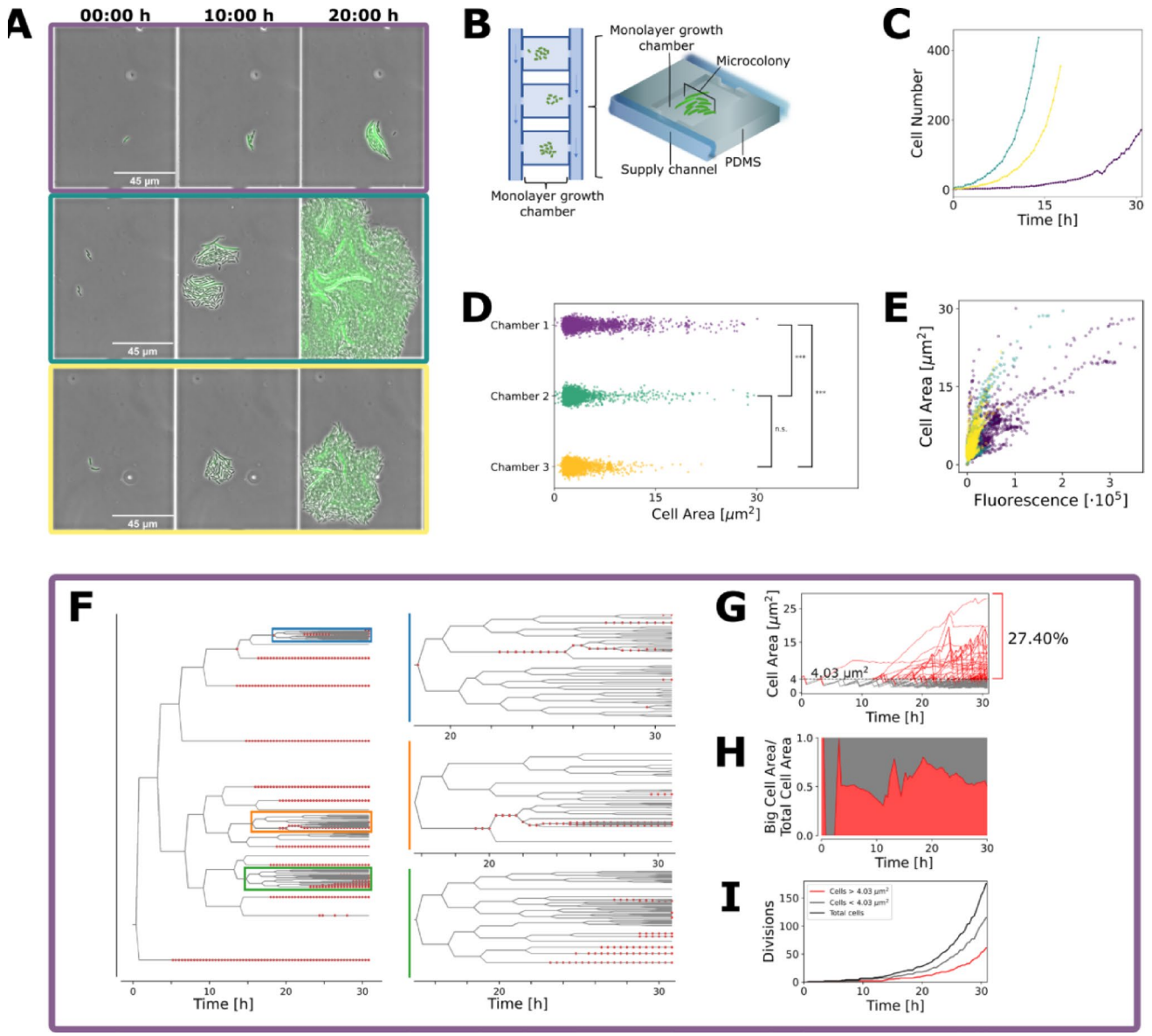


Fig. 4 Microfluidic Single-Cell cultivation of *E. coli* cells carrying a high-copy plasmid expressing GFP constitutively. **A** Live-cell imaging to monitor the cultivation of *E. coli* DH5α cells carrying a high-copy plasmid that constitutively expresses GFP inside microfluidic chambers. **B** Schematic of a section of the microfluidic chip, showing one chamber being supplied with medium via the supply channel through diffusion. **C** Number of cells in the three microfluidic chambers over time ($\mu_{max} = 0.24 \pm 0.05\ h^{-1}$). **D** Analysis of cell area, and **E** Correlation between cell area and fluorescence during the cultivation in all three chambers. **F–I** Cell tracking of the first chamber in **A**. **F** Lineage of all cells in the first chamber shown in (**A**) over time. Cells colored in red have a larger cell area than 4.03 µm², which represents the median cell area before cell division. **G** The lines represent the evolution of cell area of individual cells over time during growth and division. Cells larger than the median cell area are highlighted in red. **H** Ratio of the area covered by large cells relative to the total cell area. **I** Number of divisions per time point for cells larger and smaller than 4.03 μm^2

maintained (Fig. 5A), with the GFP-positive subpopulation consistently representing nearly 100% of the total population (Fig. 5B). Although population stability was preserved across all tested dilution rates, an increase in dilution rate was associated with a reduction in overall cell density and the onset of dissolved oxygen limitation (Fig. 5C). Furthermore, the total fluorescence intensity declined as dilution rate increased (Fig. 5A). This decline in fluorescence likely reflects a selective pressure imposed by the higher dilution rate, which may disfavor the persistence of larger, highly fluorescent cells with elevated pDNA levels (Fig. 5D). A possible influence of overflow metabolism on the yield is unlikely because acetate is only formed in small quantities at a dilution rate of 0.27 h^{-1}, and growth-inhibiting concentrations are typically reached at a dilution rate of 0.45 h^{-1} or higher [51]. These findings further support the hypothesis

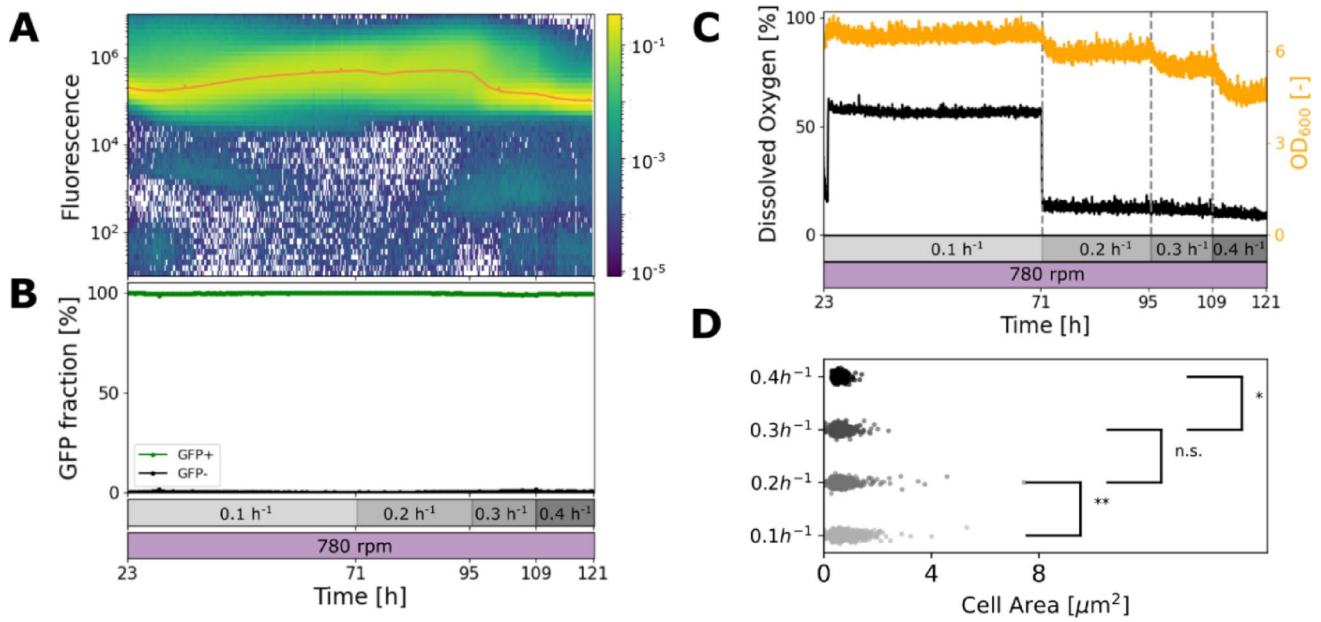


Fig. 5 A constant stirring speed of 780 rpm improves cultivation stability even with increasing dilution rates from 0.1 to 0.4 h^{-1}. **A** Fluorescence density plot of *E. coli* DH5α cells harboring a high-copy plasmid constitutively expressing GFP, cultivated at a constant stirring speed of 780 rpm with stepwise increases in dilution rate from 0.1 to 0.2, 0.3, and 0.4 h^{-1}. Each dilution rate was maintained for at least four retention times. The trend of the median fluorescence is shown as a fine red line. **B** Trend of the positive and negative fractions of cells expressing GFP (threshold = 10^4). **C** Online monitoring of dissolved oxygen and optical density during continuous cultivation and the stepwise increase in dilution rate. **D** Analyses of microscopy pictures and specifically the cell area during the cultivation at the different dilution rates. For every time point 10 pictures were made

that both mixing intensity and selective growth conditions significantly influence population structure and productivity in pDNA bioprocesses.

Mechanical stress as an important driver for population stability in continuous culture

Our data point out that there is a correlation between plasmid accumulation and cell size. Indeed, as cells accumulate pDNA, the corresponding metabolic load leads to cell elongation. Of course, these elongated cells exhibit a lower fitness, resulting in disrupted cell division and a decreased growth rate. Due to this reduced growth rate, cells with a high plasmid load tend to be washed out when the dilution rate of the continuous culture is increased (Fig. 5D). However, we observed a similar trend when different cultivation devices were used (Fig. 6). Under the laminar flow conditions met in microfluidics, large-elongated cells were allowed to proliferate. In CSTR, we observed a significant reduction in cell size as the stirrer speed was increased. Cell damage from shear stress in stirred-tank bioreactors is governed by two components i.e., the mean energy dissipation rate in the impeller swept zone and the circulation time (Fig. 6A). We estimated these components from CFD simulations and used them to compute the EDCF (equ. 4). An EDCF of 0 W kg^{-1} s^{-1} was assigned to the microfluidic experiments, since the laminar flow in these devices precludes turbulent eddies and therefore direct mechanical damage to the cells. Using this approach, we calculated a 2.9-fold increase in EDCF when the agitation speed was raised from 780 to 1000 rpm in the continuous bioreactor (Fig. 6B), pointing to a possible role of mechanical stress in the population collapse observed under the highest-EDCF condition. This effect may be partly explained by Kolmogorov's theory, which holds that cells smaller than the local turbulence length scale are less susceptible to mechanical damage in stirred-tank reactors [52, 53]. We further computed the spatial distribution of the Kolmogorov length scale from the CFD simulations (Fig. 6C, D) and found values well below the typical size of the elongated cells observed in the microfluidic experiments, particularly within the impeller swept zone. Taken altogether, these results suggest that mechanical stress acts as a part of the selective pressure between producing and non-producing cells in continuous cultures.

Discussion

High-copy plasmid maintenance imposes a strong metabolic and regulatory burden on *E. coli*, typically manifested by growth defects, SOS-induced filamentation, and altered resource allocation [1, 45]. These burden-driven

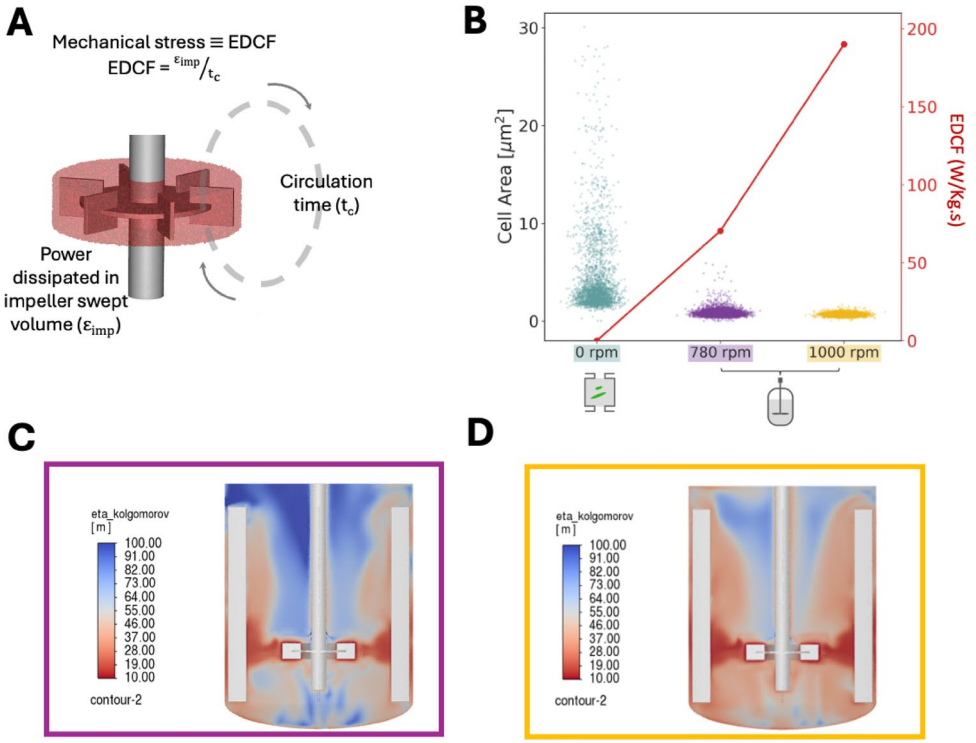


Fig. 6 Mechanical stress act as a selective pressure in continuous culture. **A** Schematic representation of the energy dissipation/circulation function (EDCF) used to quantify hydrodynamic stress, combining the power dissipated in the impeller swept volume and the circulation time. **B** Single-cell area distribution (μm²) measured by microscopy for cells cultivated in a microfluidic device under laminar flow (0 rpm) and in continuous stirred-tank bioreactors at 780 rpm and 1000 rpm agitation rate. The red line shows the corresponding EDCF (W kg^{-1} s^{-1}) computed by CFD simulations for each condition, illustrating the ~2.9-fold increase in EDCF between 780 and 1000 rpm; an EDCF of 0 W kg^{-1} s^{-1} was assigned to the microfluidic condition owing to the absence of turbulent eddies under laminar flow. **C**, **D** CFD-derived contour maps of the Kolmogorov length scale (η, μm) within the stirred-tank bioreactor at 780 rpm (**C**) and 1000 rpm (**D**), showing the reduction in the smallest turbulent eddy size with increasing agitation speed

morphological changes have an engineering consequence that is rarely considered in continuous bioprocess design i.e., an increased susceptibility to hydrodynamic stress. In stirred-tank reactors, shear tolerance is often assumed based on the Kolmogorov length scale being orders of magnitude larger than *E. coli* cell size [52]. However, our findings clearly challenge this assumption for plasmid-producing cell populations. Under high agitation in the CSTR, we observed a rapid decline of the pDNA-producing subpopulation despite maintained antibiotic selection pressure. Crucially, while plasmid retention at the kanamycin resistance locus was confirmed, this was accompanied by a marked reduction in plasmid copy number and a loss of plasmid structural integrity, suggesting that cells retained a structurally compromised or copy-depleted plasmid rather than losing it entirely. The collapse resulted in the near-complete emergence of a fast-growing GFP-negative genotype, supported by qPCR evidence of genetic alterations reducing replication burden while retaining antibiotic resistance. These results show that structural plasmid instability is the dominant escape mechanism in high-stress continuous operation.

We further demonstrate that mechanical stress dictate whether this collapse occurs based on CFD simulations. Reducing stirrer speed from 1000 to 780 rpm led to a 2.9-fold decrease in EDCF and stabilized plasmid retention for over 100 h, even at elevated dilution rates. However, automated flow cytometry and microscopy revealed a shift in cell morphology depending on the mixing intensity involved: low stirring speed allowed the persistence of large, highly fluorescent, slow-dividing cells, whereas high stirring speed suppressed this subpopulation and favored smaller, faster-growing phenotypes.

By applying stirrer-speed control as a process analytical strategy, we propose that shear tuning can be incorporated as a process parameter for maintaining pDNA stability, as well as a selection tool to modulate subpopulation ecology. Ultimately, this strategy could also be expanded as a safeguard against the emergence of plasmid-loss mutants. In practice, minimizing agitation within acceptable oxygen-transfer limits should enhance robustness, enable higher operational dilution rates, and extend production lifetime, three prerequisites for viable industrial continuous pDNA manufacturing.

Our findings uncover a previously overlooked mechano-biological coupling in plasmid DNA bioprocesses i.e., when metabolic burden causes cells to enlarge [50, 54], making them susceptible to disruptive shear forces. This physical-biological interaction promotes shear-induced evolutionary dynamics that accelerate loss of productive genotypes and ultimately drive population collapse. Importantly, we demonstrate that controlling agitation is a simple, scalable intervention capable of stabilizing productive subpopulations and preserving plasmid integrity during continuous bioproduction.

Despite its significance, the mechanobiology of *E. coli* remains poorly understood [55], especially under production stress. While microbial responses to extracellular stress have been studied, primarily in the context of antibiotics [56], and shear responses are well characterized in higher eukaryotes such as CHO cells [53], most microbial mechanobiology has been examined through surface-dependent processes like biofilm formation [57]. Virtually no studies have explored how fluid-dynamic stresses shape subpopulation behaviors in planktonic, industrially relevant cultures. Bridging this knowledge gap will be essential to engineer robustness in next-generation continuous bioprocesses, where metabolic burden and hydrodynamic stress intersect to dictate evolutionary fate.

Supplementary Information The online version contains supplementary material available at https://doi.org/10.1007/s00449-026-03433-4.

Acknowledgements The authors thank Alexander Grünberger's lab (Karlsruhe Institute of Technology), especially Boris Yermakov, for providing the PDMS chips that were used to perform microfluidic experiments. The authors acknowledge the excellent technical assistance from Andrew Zicler and Samuel Telek (ULiège).

Author contributions Concept and design of the study: HS, FD, RK. Acquisition of data: HS, JAM, RK, MD, MA. Analysis and interpretation of results: HS, JAM, RK, MD, MA, FD.

Funding This work was sponsored by GlaxoSmithKline Biologicals SA.

Data availability No datasets were generated or analysed during the current study.

Declarations

Conflict of interest This work was sponsored by GlaxoSmithKline Biologicals SA. RK and MA are employees of the GSK group of companies.

References

1. Silva F, Queiroz JA, Domingues FC (2012) Evaluating metabolic stress and plasmid stability in plasmid DNA production by *Escherichia coli*. Biotechnol Adv 30:691–708
2. Flores S, de Anda-Herrera R, Gosset G, Bolívar FG (2004) Growth-rate recovery of *Escherichia coli* cultures carrying a multicopy plasmid, by engineering of the pentose-phosphate pathway. Biotechnol Bioeng 87:485–494
3. Ow DS-W, Nissom PM, Philp R, Oh SK-W, Yap M (2006) G.-S. Global transcriptional analysis of metabolic burden due to plasmid maintenance in *Escherichia coli* DH5α during batch fermentation. Enzym Microb Technol 39:391–398
4. Wang Z, Xiang L, Shao J, Wegrzyn A, Wegrzyn G (2006) Effects of the presence of ColE1 plasmid DNA in *Escherichia coli* on the host cell metabolism. Microb Cell Fact 5:34
5. Li Z, Rinas U (2020) Recombinant protein production associated growth inhibition results mainly from transcription and not from translation. Microb Cell Fact 19:83
6. Rozkov A et al (2004) Characterization of the metabolic burden on *Escherichia coli* DH1 cells imposed by the presence of a plasmid containing a gene therapy sequence. Biotechnol Bioeng 88:909–915
7. Little JW, Mount DW (1982) The SOS regulatory system of *Escherichia coli*. Cell 29:11–22
8. Maslowska KH, Makiela-Dzbenska K, Fijalkowska IJ (2019) The SOS system: a complex and tightly regulated response to DNA damage. Environ Mol Mutagen 60:368–384
9. Oliveira PH, Prather KJ, Prazeres DMF, Monteiro GA (2009) Structural instability of plasmid biopharmaceuticals: challenges and implications. Trends Biotechnol 27:503–511
10. Popov M, Petrov S, Nacheva G, Ivanov I, Reichl U (2011) Effects of a recombinant gene expression on ColE1-like plasmid segregation in *Escherichia coli*. BMC Biotechnol 11:18
11. Reinikainen P et al (1989) *Escherichia coli* plasmid production in fermenter. Biotechnol Bioeng 33:386–393
12. Grijalva-Hernández F et al (2019) High kanamycin concentration as another stress factor additional to temperature to increase pDNA production in *E. coli* DH5α batch and fed-batch cultures. Microorganisms 7:711
13. Wegrzyn G (1999) Replication of plasmids during bacterial response to amino acid starvation. Plasmid 41:1–16
14. Wróbel B, Wegrzyn G (1997) Replication and amplification of lambda plasmids in *Escherichia coli* during amino acid starvation and limitation. FEMS Microbiol Lett 153:151–157
15. Horn U, Krug M, Sawistowski J (1990) Effect of high density cultivation on plasmid copy number in recombinant *Escherichia coli* cells. Biotechnol Lett 12:191–196
16. Prather KJ, Sagar S, Murphy J, Chartrain M (2003) Industrial scale production of plasmid DNA for vaccine and gene therapy: plasmid design, production, and purification. Enzym Microb Technol 33:865–883
17. O'Kennedy RD, Baldwin C, Keshavarz-Moore E (2000) Effects of growth medium selection on plasmid DNA production and initial processing steps. J Biotechnol 76:175–183
18. Götting C, Thierbach G, Pühler A, Kalinowski J (1998) Versatile low-copy-number plasmids for temperature-inducible overexpression of bacterial genes in *Escherichia coli*. Biotechniques 24:362–364
19. Friehs K (2004) Plasmid copy number and plasmid stability. Adv Biochem Eng Biotechnol 86:47–82
20. Wang Z, Le G, Shi Y, Węgrzyn G (2001) Medium design for plasmid DNA production based on stoichiometric model. Process Biochem 36:1085–1093

21. Wang Z, Le G, Shi Y, Wegrzyn G, Wrobel B (2002) A model for regulation of ColE1-like plasmid replication by uncharged tRNAs in amino acid-starved *Escherichia coli* cells. Plasmid 47:69–78
22. Gotsmy M et al (2023) Sulfate limitation increases specific plasmid DNA yield and productivity in *E. coli* fed-batch processes. Microb Cell Fact 22:242
23. Lara AR, Jaén KE, Folarin O, Keshavarz-Moore E, Büchs J (2019) Effect of the oxygen transfer rate on oxygen-limited production of plasmid DNA by *Escherichia coli*. Biochem Eng J 150:107303
24. O'Mahony K, Freitag R, Hilbrig F, Müller P, Schumacher I (2007) Strategies for high titre plasmid DNA production in *Escherichia coli* DH5a. Process Biochem 42:1039–1049
25. Yanisch-Perron C, Vieira J, Messing J (1985) Improved M13 phage cloning vectors and host strains: nucleotide sequences of the M13mp18 and pUC19 vectors. Gene 33:103–119
26. Rouches MV, Xu Y, Cortes LBG, Lambert G (2022) A plasmid system with tunable copy number. Nat Commun 13:3908
27. Jaén KE, Velázquez D, Sigala J-C, Lara AR (2019) Design of a microaerobically inducible replicon for high-yield plasmid DNA production. Biotechnol Bioeng 116:2514–2525
28. Seo JH, Bailey JE (1986) Continuous cultivation of recombinant *Escherichia coli*: Existence of an optimum dilution rate for maximum plasmid and gene product concentration. Biotechnol Bioeng 28:1590–1594
29. Henrion L et al (2023) Fitness cost associated with cell phenotypic switching drives population diversification dynamics and controllability. Nat Commun 14:6128
30. Nguyen TM et al (2021) Reducing phenotypic instabilities of a microbial population during continuous cultivation based on cell switching dynamics. Biotechnol Bioeng 118:3847–3859
31. Croughan MS, Hamel J-F, Wang D (1987) I. C. Hydrodynamic effects on animal cells grown in microcarrier cultures. Biotechnol Bioeng 29:130–141
32. Iurashev D et al (2024) Scaling strategy for cell and gene therapy bioreactors based on turbulent parameters. Biotechnol J 19:2300235
33. Segall-Shapiro TH, Sontag ED, Voigt CA (2018) Engineered promoters enable constant gene expression at any copy number in bacteria. Nat Biotechnol 36:352–358
34. Täuber S et al (2021) How to perform a microfluidic cultivation experiment-A guideline to success. Biosensors 11
35. Stringer C, Wang T, Michaelos M, Pachitariu M (2021) Cellpose: a generalist algorithm for cellular segmentation. Nat Methods 18:100–106
36. Cutler KJ et al (2022) Omnipose: a high-precision morphology-independent solution for bacterial cell segmentation. Nat Methods 19:1438–1448
37. Ershov D et al (2022) TrackMate 7: integrating state-of-the-art segmentation algorithms into tracking pipelines. Nat Methods 19:829–832
38. Tinevez J-Y et al (2017) TrackMate: An open and extensible platform for single-particle tracking. Methods 115:80–90
39. Liu Y et al (2016) Application of Euler Lagrange CFD for quantitative evaluating the effect of shear force on Carthamus tinctorius L. cell in a stirred tank bioreactor. Biochem Eng J 114:209–217
40. Nienow AW (2021) The impact of fluid dynamic stress in stirred bioreactors – the scale of the biological entity: a personal view. Chem Ing Tech 93:17–30
41. Antognoli M et al (2025) Power and fluid stress in disposable square stirred tank to streamline pharmaceutical process development. Int J Pharm 685:126243
42. Csibra E, Stan G-B (2022) Absolute protein quantification using fluorescence measurements with FPCountR. Nat Commun 13:6600
43. Shao B et al (2021) Single-cell measurement of plasmid copy number and promoter activity. Nat Commun 12:1475
44. Summers DK (1991) The kinetics of plasmid loss. Trends Biotechnol 9:273–278
45. Snoeck S, Guidi C, De Mey M (2024) Metabolic burden' explained: stress symptoms and its related responses induced by (over)expression of (heterologous) proteins in *Escherichia coli*. Microb Cell Fact 23:96
46. Haddadin FT, Harcum SW (2005) Transcriptome profiles for high-cell-density recombinant and wild-type *Escherichia coli*. Biotechnol Bioeng 90:127–153
47. Täuber S, Golze C, Ho P, von Lieres E, Grünberger A (2020) dMSCC: a microfluidic platform for microbial single-cell cultivation of Corynebacterium glutamicum under dynamic environmental medium conditions. Lab Chip 20:4442–4455
48. Campos M et al (2014) A constant size extension drives bacterial cell size homeostasis. Cell 159:1433–1446
49. Wehrens M et al (2018) Size laws and division ring dynamics in filamentous *Escherichia coli* cells. Curr Biol 28:972–979e5
50. Silva F, Passarinha L, Sousa F, Queiroz JA, Domingues FC (2009) Influence of growth conditions on plasmid DNA production. J Microbiol Biotechnol 19:1408–1414
51. Valgepea K et al (2010) Systems biology approach reveals that overflow metabolism of acetate in *Escherichia coli* is triggered by carbon catabolite repression of acetyl-CoA synthetase. BMC Syst Biol 4:166
52. Hewitt CJ, Boon LA, McFarlane CM, Nienow AW (1998) The use of flow cytometry to study the impact of fluid mechanical stress on *Escherichia coli* W3110 during continuous cultivation in an agitated bioreactor. Biotechnol Bioeng 59:612–620
53. Papoutsakis ET (1991) Fluid-mechanical damage of animal cells in bioreactors. Trends Biotechnol 9:427–437
54. Silva F, Lourenço O, Maia C, Queiroz JA, Domingues FC (2011) Impact of plasmid induction strategy on overall plasmid DNA yield and *E. coli* physiology using flow cytometry and real-time PCR. Process Biochem 46:174–181
55. Harper CE, Hernandez CJ (2020) Cell biomechanics and mechanobiology in bacteria: challenges and opportunities. APL Bioeng 4:021501
56. Yang DC, Blair KM, Salama NR (2016) Staying in shape: the impact of cell shape on bacterial survival in diverse environments. Microbiol Mol Biol Rev 80:187–203
57. Dufrêne YF, Persat A (2020) Mechanomicrobiology: how bacteria sense and respond to forces. Nat Rev Microbiol 18:227–240

Publisher's Note Springer Nature remains neutral with regard to jurisdictional claims in published maps and institutional affiliations.

Springer Nature or its licensor (e.g. a society or other partner) holds exclusive rights to this article under a publishing agreement with the author(s) or other rightsholder(s); author self-archiving of the accepted manuscript version of this article is solely governed by the terms of such publishing agreement and applicable law.